Journal of Materials Chemistry B

Accepted Manuscript

ROYAL SOCIETY OF CHEMISTRY

www.rsc.org/materialsB

Bone cement based nanohybrid as super biomaterial for bone healing

Govinda Kapusetti[1], Nira Misra[1], Vakil Singh[2], Swati Srivastava[3], Partha Roy[3], Kausik Dana[4] and Pralay Maiti[5,*]

[1]School of Biomedical Engineering, Indian Institute of Technology (Banaras Hindu University), Varanasi 221 005, India.

[2]Department of Metallurgical Engineering, Indian Institute of Technology (Banaras Hindu University), Varanasi 221 005, India

[3]Department of Biotechnology, Indian Institute of Technology Roorkee 247667 Roorkee 247667, India

[4]Central Glass and Ceramic Research Institute, Kolkata 700 032, India

[5]School of Materials Science and Technology, Indian Institute of Technology (Banaras Hindu University), Varanasi 221 005, India

* To whom correspondence should be addressed
Email: pmaiti.mst@itbhu.ac.in (P. Maiti)

Abstract

Novel bone cement based nanohybrid has been developed which is capable of healing the fractured bone in one-third time (in 30 days) than that of natural healing process. Nanohybrids of poly(methyl methacrylate) (PMMA) based bone cement, being used as grouting material in joint replacement surgeries, with organically modified layered silicates of varying chemical compositions have been prepared by simple mixing. It exhibits considerably low temperature, reduced by 12^{o}C, arising from exothermic polymerization, and thereby, circumvents the reported cell necrosis during implantation using pure bone cement. The thermal stability and mechanical superiority have been verified through higher degradation temperature, better stiffness, superior toughness and significantly higher fatigue resistance behavior of nanohybrid vis-à-vis pure bone cement to make it appropriate for implant material. The biocompatibility and bioactivity have been confirmed using cell adhesion, cell viability and fluorescence image to understand the cell health on different materials and have been compared for their suitability. Osteoconductivity and bone bonding ability have been monitored in vivo on rabbits through radiographic imaging and histopathology of growing bone and muscle near the surgery site. The observed dissimilarity of properties in two different nanoclays as fillers have been visualized through interaction as measured by using spectroscopic techniques and elemental influence on bioactivity exhibiting higher efficiency for greater iron containing nanoclay.

Key words: Bone cement, nonohybrid, biocompatibility/bioactivity, fatigue, bone healing

INTRODUCTION

Poly(methyl methacrylate) (PMMA) bone cement (hereafter referred to as, "bone cement") has been used in joint surgeries since the pioneering efforts of Sir. Jhon Charnley in 1958.[1] Bone cement has many attractive properties, such as easy preparation and handling, rapid self-hardening, and excellent biocompatibility. However, bone cement has a number of shortcomings, such as high exothermic temperature during polymerization (up to 100 ^{o}C, in some cases), which may cause thermal necrosis of peri-prosthetic tissue which, in turn, may play a role in aseptic loosening of the implant;[2,3] poor adhesion to the contiguous bone (bio-inertness),[4,5] which leads to generation of a gap between the bone and the cement, which may contribute to implant failure; inadequate mechanical properties,[6,8] such as fatigue strength; and lack of bioactivity.

Over the years, there have been many reports on experimental bone cement formulations that address the aforementioned and other shortcomings of the current generation of approved cement brands. Among these efforts is reinforcement of the cement matrix through incorporation of a filler in the cement powder, examples of fillers being nano-sized BaSO4 particles,[9] multi-walled carbon nanotubes,[10] calcium acetate particles,[11] β-tricalcium phosphate (β-TCP) particles encapsulated with poly(ethylene glycol),[12] oligomer,[13] polyethylene fibers,[14] carbon fibers,[15,16] hydroxyapatite (HA) particles,[17] glass fibers,[18] graphite fibers,[19] and nanoclay.[20] Another approach involved using bone cement/layered double hydroxide (LDH) nanohybrids.[21,22] Some of the reinforcing fillers, such as HA particles. β-TCP particles, and nanoclay, as well as LDH nanohybrids also impart bioactivity to the bone cement. There are many literature reports on bone cement/nanoclay composites,[20,23-27] as well as on general-purpose PMMA/clay composites,[28-32] with results including many aspects, such as mechanical properties, effect of synthesis method on structural properties, and degradation in various media. The chemical

modification over the surface of the nanoclay platelets has a significant role as organic modification makes the surface suitable for its interaction with matrix polymer. The improvement in properties thereby predominantly depends on the organic modifier used for the nanoclay modification. However, in the case of bone cement/nanoclay composites, information is lacking on the influence of composition of the clay, in particular its Fe and Mg ion contents, on properties of the composite as well as on the fatigue properties, in vitro biocompatibility, and in vivo performance of the composites.

In the present work, bone cement/ layered silicate nanohybrids have been prepared with varying mineral compositions and thereby the CEC of nanoclay and extreme diverse organic modifications to cater the differences. The improved thermal and mechanical properties especially the fatigue behavior has been tested and found suitable for its real use as grouting material for total arthroplasty surgery. The bioactivity and total biocompatibility have been examined using human osteoblast like cells (MG-63) through cell adhesion, cell viability assays and compared with the relative bioactive nature of pure bone cement and its nanohybrids. The efficacy of nanohybrid towards bone healing has been verified using them as implant in vivo in rabbit through radiographic imaging. The highly dissimilar behavior of two different nanoclays and paradigm improvement using particular nanoclay has been understood in terms of interaction and subsequent testing with cell biology taking individual chemical species separately.

MATERIALS AND METHODS

Materials: An approved PMMA bone cement brand (CMW-1; Johnson & Johnson DePuy, Warsaw, IN, USA) was used as the control cement. The cement is a two-pack system, one pack

containing the powder and the other the liquid monomer. Two different types of organically modified nanoclays , based on montmorillonite, were used: (i) 30B ion-exchanged with methyl tallow bis-hydroxyethyl quaternary ammonium (cation exchange capacity (CEC) = 100 meq/100 g; Southern Clay, Gonzales, TX, USA); and (ii) NK75 (ion-exchanged with dimethyl dihydrogenated tallow ammonium; CEC = 70 meq/100 g, Indian origin high iron content MMT, where tallow contains ~65 % C_{18}; ~30 % C_{16}; ~5 % C_{14}.[33] The elemental compositions of the two nanoclays were determined using EDAX (200FEG, FESEM Quanta) showing 2.5 and 2 wt.% of Mg and Fe in 30B and 0.9 and 8 wt.% of Mg and Fe in NK75 nanoclay, respectively (Fig. 1).

Preparation of bone cement and nanohybrids: The control cement (herein designated BC cement) was prepared by hand mixing the powder and the liquid in a bowl with a glass rod for 2 min at room temperature (temperature and relative humidity of ~24 ^{o}C; and 40 ± 15 %, respectively). The nanohybrids (herein designated BC-B and BC-N composites) were prepared by using 30B / NK75 nanoclays taking 0.5, 1, 1.5 and 2 wt%. The powder part of the control cement and the selected amount of the respective nanoclay were mixed in an electronic mixer, operated at 2000 rev/min, for 15 min, after which the blend was mixed with the liquid monomer of the control cement, as detailed above.

Spectroscopic examinations: Ultra-violet (UV)-visible spectroscopy measurements were carried out by using Shimadzu (*UV-1700*), Pharma Speck, *UV–Vis* spectrophotometer operating in the spectral range of 200–1100 nm. Three transparent thin films of each cement with thickness ~30 µm were prepared through solution route by dissolving in THF (tetrahydrofuran) as the solvent followed by evaporation of the solvent on a quartz glass. Fourier transform infra-red (FTIR) spectroscopy was used to detect the functional groups of the nanoclays and to understand

the nature of the interaction between the cement matrix and the nanoclay. FTIR was performed in transmission mode at room temperature from 400-4000 cm^{-1} (Nicolet 670), with a resolution of 4 cm^{-1} with taking bubble free thin films.

Thermal and handling characterization: Thermal stability was examined using thermo gravimetric analyzer (*TGA*) (Mettler-Toledo) fitted with differential thermal analyzer (*DTA*). Data were taken from 40 – 550 °C. All the experiments were performed at a heating rate of 20°C min^{-1} in a nitrogen atmosphere. The glass transition temperature (T_g) was determined using differential scanning calorimetry (Mettler 832), at a heating rate of 10 ^oC/min with one sample of each cement, respectively. The calorimeter was calibrated using indium. The maximum exotherm (T_{max}) and the setting time (t_{set}) were measured following the method described in the relevant ASTM standards.[34] T_{max} was measured with a thermocouple which was placed in the cement dough (Selec, DTC 503, Mumbai, India) and t_{set} was taken at the point halfway between the ambient temperature and the peak temperature. These measurements were carried out for three times for each cement.

Mechanical properties: The modulus of elasticity (E) and toughness were determined using dog-bone shaped specimens, prepared by a compression molding technique, and a universal testing machine (Instron 3369). The tests were carried out in air, at a crosshead displacement rate of 5 mm/min. Toughness was computed as the area under the stress-strain curve up to failure point. For each of the cements three specimens were used.

Fatigue tests: BC, 1 wt% BC-B, and 1 wt% BC-N cements were used. The tests were carried out on a construct comprising a femoral stem of total hip implant inserted in a human male femur. The femurs were collected from the Institute of Medical Sciences, Banaras Hindu University, Varanasi, and the stems (Co-Cr alloy) were purchased from ORMAD Medical Technologies,

Ltd., Bangalore, India. The tests were performed using a materials testing machine (Model 810; MTS; 50 kN capacity). In a test, the load was applied at 45^{o} to the top of the joint (to mimic the clinical situation), at a frequency of 3 Hz.[35] The loads used were ± 1.0 kN, ± 1.5 kN, ± 2.0 kN, ± 2.5 kN, ± 3.0 kN, ± 3.5 kN, ± 4.0 kN, and ± 4.5 kN. Loading continued either 50,000 cycles were completed or the specimen fractured, whichever occurred first. If a specimen fractured, the number of load cycles at which this occurred was recorded. In another series of tests, BC, 1 wt% BC-B, and 1 wt% BC-N specimens and a load of ± 3.5 kN were used. The test continued until the specimen fractured. In each of the two series of tests, for each cement, three specimens were used.

Morphology of fracture surfaces: The morphology of the surfaces of fractured specimans from the second series of fatigue tests was obtained using scanning electron microscope (SEM). Prior to an SEM examination, a sputtering unit (SPRA 40; Zeiss Instruments), operated at 10 kV, was used to coat the specimen with a gold layer and two specimens were used for each cement for these examination.

Hemolysis assay: The assay was carried out on BC, 1 wt% BC-B, and 1 wt% BC-N specimens with triplicate samples in acid citrate dextrose (ACD) human blood.[21] 5ml of ACD blood was prepared by adding 4.5 ml of fresh human blood to 0.5 ml ACD. The ACD solution was prepared by mixing 0.544 g of anhydrous citric acid, 1.65 g of trisodium citrate dehydrate, and 1.84 g of dextrose monohydrate in 75 ml of distilled water. Equal weight of haparised films of bone cement or its nanohybrids were taken in different test tubes. 10 ml phosphate buffer solution (PBS) solution was added to both the test tubes and 10ml distilled water and 10ml PBS solution was taken in other test tubes for positive control and negative controls, respectively. All these test tubes were kept in desiccators for 30min at 37 ^{o}C. The test tubes were centrifuged for 8min

at 5000 rpm. Optical density (OD) of the thin films, the positive control, and the negative control were measured, at 545 nm, from 1 mL supernatant. The hemolysis % was calculated as follows:

$$\%\,of\ hemolysis = \frac{OD\,of\ the\ test\ sample - OD\,of\ the\ negative\ sample}{OD\,of\ the\ positive\ sample - OD\,of\ the\ negative\ sample}\ X\,100$$

Cell culture studies: BC, 1 wt% BC-B, and 1 wt% BC-N specimens (measuring 10 mm × 10 mm × 4 mm) were used. A Teflon sheet of 4 mm thickness was molded with male-female puncture system and the molds were smoothened with emery paper. The specimens were injected in to square-shaped Teflon sheet cavities and the injected Teflon mold was clamped with vice for 10 min and covered with two plain Teflon sheets above and beneath. The cured specimens were removed from the molds and the edges were smoothened with emery paper and the specimens were stored at room temperature. Before performing the cell studies, the specimens were washed with isopropanol for removing the attached debris. For surface sterilization, each specimen was washed thrice with phosphate buffered saline (pH~7.2), and exposed under UV light for 8 h. Cement extracts (cement leached medium) were then prepared for microscopic analysis of cellular structures. In accordance with ASTM standards, the weight/volume of the cement specimen and of the medium was kept at 1 g/5ml for an incubation period of 72 h. The specimen incubated in minimum essential medium (MEM) at 37 °C for 72 h in glass containers. Upon completion of the incubation period, the extracts were collected and stored at -20 °C. Different concentrations of Fe (2, 6 and 8 %) and Mg (1, 3 and 5 %) solutions were prepared in 1ml culture medium with $FeCl_3$ and $MgCl_2$, respectively, and these solutions were used for MTT assay and apoptosis study.

Cell culture: MG-63 is an established cell line of osteoblast-like cells. It was obtained from the National Centre for Cell Sciences, Pune, India (Ref. No. CREP696). The cells were cultured in MEM supplemented with heat-inactivated fetal calf serum (10 %) (Invitrogen Carlsbad, CA,

USA), penicillin (100 U/ml), streptomycin (100 U/ml) and gentamicin (20 µg/ml) (Sigma, St, Louis, MO, USA) at 37 °C in a humidified CO_2 incubator maintained at 5 % CO_2.

Cell attachment: The cell attachment behavior of MG-63 cell line to the bone cement and its 1wt% nanohybrids was evaluated through the modified crystal violet staining assay protocol.[36] For this assay, 1×10^5 cm^{-2} cells to the surfaces of BC, 1 wt% BC-B, and 1 wt% BC-N specimens with triplicate was incubated for 4 h to examine the cell attachment properties of the matrix. After 4 h, the incubated specimens were washed with PBS to remove the unattached cells and then the attached cells were fixed ice-cold 4 % paraformaldehyde (Sigma) for 20 min. Cell permeabilisation was carried out with 20 % methanol for 20 min after PBS washing. The attached cells were then stained by exposure to 0.5 % crystal violet aqueous solution (Raymond Lamb, Loughborough, UK) for 30 min. Excess stains were removed by three gentle washes in deionised water, followed by elution of the residual crystal violet with 10 % acetic acid for 30 min during gentle agitation on an elliptical shaker. OD of the eluted solution was measured in UV-Vis spectrophotometer (Double Beam LI-2800; Lasany, Chandigarh, India), at a wavelength of 570 nm, with the background absorbance value measured at 650 nm. The OD values were directly correlated with the number of attached cells.

Cell viability: Cell viability was measured by MTT (4, 5-dimethylthiazol-2-yl-2, 5-diphenyl tetrazolium bromide) assay.[22] For this assay, 1×10^5 /cm^2 MG-63 cells were seeded on the cement specimens in 24-well culture plates with triplicate in 1 mL MEM. Similarly, 1 mL of Fe (2, 6 and 8 %) and Mg (1, 3 and 5 %) solutions were added to culture plates and incubated for 24, 48 and 72 h time intervals at 37 °C. Following this treatment, 50 µL of 5 mg/ml MTT solution was added to the wells and incubated for another 4 h at 37 °C to form formazan. The MTT-containing medium was then aspirated and 100 µL of DMSO (Himedia, Mumbai, India)

were added to it to solubilize the water-insoluble formazan. Absorbance was measured using a UV-Vis spectrophotometer (Double-Beam LI-2800), at 570 nm. The % cell viability was calculated using the following formula.

$$\%\ of\ cell\ viability = \frac{OD\ of\ T}{OD\ of\ C} \times 100$$

where, C= optical density of 'control' represents osteoblasts incubated in medium alone and T = optical density of test specimen representing osteoblasts treated with corresponding extracts.

Cell proliferation: The extracts of each of the cements and different concentrations of Fe and Mg solutions were visually examined to characterize cell proliferation using fluorescence microscopy after 24 h of incubation. The MG-63 cells were suspended in fresh complete medium, at a density of 0.5 × 105 cells/mL in a 96-well of triplicate and were incubated for 4h. After the initial incubation, 0.2 mL extracted medium was replaced with fresh medium in each well except the control and finally incubated for 24 h. Cells were washed with PBS, stained with propidium iodide for cement/nanohybrids and 0.5µg/mL working concentration of DAPI was used for metal ions (Fe and Mg). After that, these solutions were incubated in a dark place for 30 min at room temperature. Imaging was performed using a fluorescence microscope (Nikon Eclipse 80i; Nikon, Buckinghamshire, UK).

Apoptosis: Cells were incubated in 100µl of media for 1 day in a 90-well plate in triplicate after one day incubation 5µl of Fe (2, 6 and 8 %) and Mg (1, 3 and 5 %) sample media were added to the cultured wells. After that, these solutions were incubated for 1 day, followed by 1:1 concentration (100 µg/mL) of acridin orange and ethidium bromide solution was used to stain the cells for 2 min. Imaging was performed using a fluorescence microscope (Nikon Eclipse 80i).

***In vivo* studies:** A total of 48 male rabbits, each weighing 2.5 – 3.0 kg, were procured from the Animal Care Unit, Centre Experimental Medicine and Surgery, Institute of Medical Sciences,

Banaras Hindu University, Varanasi, after getting permission from the Institutional Ethics Committee (see No. Dean/12-13/CAEC/25). Four groups of specimens (blank, BC, BC-B, and BC-N) were implanted in 12 rabbits each (6 to be used for X-rays and 6 for histopathology). For the surgery, the rabbit was anesthetized using intra peritoneal injections of ketamine hydrochloride (1 mg/kg), 1 mg/kg of medazolam supplemented with local 2 % xylocane with adrenaline 1:1000 under standard condition of animal care guideline. The right tibia of fully anesthetized rabbit was washed with iodine tincture (Betadine 10% aqueous) followed by alcohol (70 %). One cavity was made in right tibia with 4 mm diameter and 8 mm depth using a hand drill. Rabbits of group 2, 3 and 4 were injected with BC, 1 wt% BC-B, and 1 wt% BC-N, respectively, while group 1 was taken as control (without any material). The incision area was covered by micro pore with 3-5 stitches. The drilled hole and the image after filling the hole of the tibia of rabbit with cement/nanohybrids have been shown in supporting document (Supplementary Figure 3). Digital X-ray radiography (Shimadzu RAD Speed, at 41 kV) was used to obtain X-ray images every 5 days starting with the day of surgery. Radiographs were taken of the proximal metaphyseal, the diaphyseal region, and the distal metaphyseal. Based on the X-ray results, two rabbits of each group were scarified for histopathology assessment.

Histopathology: BC, BC-B, and BC-N specimens were fixed with 10wt% formaldehyde solution. Dehydrated and decalcified bone samples were embedded in paraffin and three slices are made with microtome of thickness around 10-15 µm. Similarly, 5µm slices were prepared for soft tissue samples. Histological evaluation was performed on hematoxylin and eosin stained sections. After the radiographic examination, the rabbits were sacrificed. In each of the sacrificed rabbit, the implanted zones (bone and muscle) were preserved, consistent with normal practice.

Statistical analysis: The results are expressed as mean ± standard deviation. In terms of test of significance, 1) results of T_{max}, tensile modulus, toughness and fatigue tests were analyzed using ANOVA followed by post-hoc Dunnett's multiple comparison test, 2) results from the hemolysis assay and cell viability tests were analyzed using ANOVA followed by post-hoc Dunnett's multiple comparison test and by post-hoc Bonferroni test, respectively, and 3) results from the cell attachment tests were analyzed using ANOVA followed by post-hoc hoc Dunnett's multiple comparison test; (GraphPad Prism 5,1). Significance was denoted as $p < 0.05$. The absence of p values indicates their insignificant nature.

RESULTS AND DISCUSSIONS

Maximum exothermic (T_{max}) temperature, setting time (t_{set}) and interactions:

Bone cement and its nanohybrids have been prepared at room temperature; exothermic temperature has been measured as a function of time during polymerization, with three reputations. During polymerization maximum exothermic temperature of pure bone cement was found around (T_{max}) of 84 ± 1.4 ^{o}C and setting time was 7 minutes, while higher temperature by 4 ^{o}C was exhibited in BC-B nanohybrid (Fig. 2a). On the contrary, the T_{max} for BC-N nanohybrid was 72 ± 1.2 ^{o}C, nearly 12 ^{o} C ($p < 0.001$) less than that of pure bone cement indicating better material for use in implant. There was no significant difference in the t_{set} results: 7 ± 0.45 min, 7.5 ± 0.45 min and 7 ± 0.30 min for BC, BC-B and BC-N, respectively (Fig. 2a). It has potential to reduce cell necrosis at bone cement-bone interfaces because of relatively lower temperature,[37] along with its lowest slope of temperature increasing trend. However, BC-N nanohybrid has largely reduced the exothermic temperature generated from polymerization reaction and, thereby, minimizes the possible cell death.

In order to understand the considerable lowering of temperature for BC-N, the interaction between polymer matrix and nanofillers have been worked out through spectroscopic techniques. The sharp carbonyl stretching frequency of the acrylate group appears at 1728 cm^{-1} for pure bone cement which remains unaffected for BC-B while significant shifting occurs to 1718 cm^{-1} for BC-N strongly supports the better interaction between PMMA moiety in bone cement with NK-75 nanofiller (Fig. 2b). The transmission peaks of other functional group in bone cement appeared at 1144 cm^{-1} to 1243 cm^{-1} is due to the stretching vibration of C–O–C bond, at 1441 cm^{-1} of bending vibration of the C–H bonds of the $–CH_3$ groups and one weak transmittance peak appears at 3,437 cm^{-1} due to the O–H stretching.[38] The transmittance peaks corresponding to –CH3 group appears at 1443 cm^{-1} in pure bone cement which has shifted towards lower wavelength region (1431 cm^{-1}) in BC-N while it remained unchanged for BC-B nanohybrid. In addition, some new peaks appear in nanohybrids at 2848 cm^{-1} ($-CH_2-$) and 1060 cm^{-1} (Si-O) revealing presence of nanoclay and the intensity of these peaks increase for higher clay content nanohybrids. Similarly, a hump in the UV absorption range at 225 nm, assigned for $n \rightarrow \sigma^*$ transition ,[39] for pure bone cement has shifted to 228 and 234 cm^{-1} (red shift) for BC-B and BC-N, respectively, auxiliary indicates stronger interaction in BC-N (greater shift) as compared to BC-B nanohybrid (Fig. 2c). Moreover, a peak at 277 nm, due to $\pi \rightarrow \pi^*$ transition,[40] has shifted to 279 and 280 cm^{-1} for BC-B and BC-N, respectively, again indicate considerable interaction in BC-N as compared to BC-B nanohybrid. UV-Vis spectra of different nanoclays are shown in inset of Figure 2c in the wavelength range of 200-600 nm. The red shift of about $\Delta\lambda_{max}$ = 9 nm suggests that NK75 clay withdraw the electron cloud from the carbonyl group of PMMA in bone cement,[41] the analogous observation also found in FTIR studies. However, the interaction between NK75 and bone cement is quite strong as evident from the peak shifting in FTIR and

UV-Vis studies as compared to BC-B nanohybrid suggesting better energy dissipating mechanism in BC-N and thereby reducing the rise of temperature through greater interactions and expected to improve the other properties accordingly as reported in strongly interacted PMMA/MMT nanocomposite for electrical and electrochemical applications.[42] The greater interaction is reflected in the exfoliated nanostructure in BC-N as revealed from the good dispersed bright field TEM image and absence of any (001) basal reflection in XRD profile against the stacked layered silicate in TEM micrograph and the presence of (001) reflection in the XRD pattern of BC-B nanohybrid (Supplementary Fig. S1).

Thermal degradation temperature (T_{deg}) and glass transition temperature (T_g):

Thermal stability of pure bone cement and its nanohybrids have been compared by monitoring its weight as a function of temperature in thermogravimetric analyzer (Fig. 2d). The T_{deg} of a polymer / composite is taken as the temperature corresponding to 5 % weight loss. The T_{deg} of pure bone cement, BC-B and BC-N were found to be 454 ± 3, 245 ± 3 and 262 ± 3 ^{o}C, respectively, (horizontal line in the inset figure of Fig. 2d) indicating better thermal stability of the BC-N as compared to pure bone cement and BC-B nanohybrid by creating thermal barrier in presence of homogeneously dispersed layered silicate (NK75) in bone cement matrix. On the other hand, lesser interaction and stacked nanoclay pattern in BC-B nanohybrid leads to the lowering of degradation temperature in comparison with pure bone cement. Thermal stability of PMMA / MMT hybrid is srongly corelated to their mixing; exfoliated nanohybrids is highly stable as compared to intercalated one,[43,44] and further, the degradation temperature of nanohybrid increases with increasing nanoclay content in case of exfoliated system, but this trend is not observed in intercalated hybrids. Hence, the thermal stability has enhanced in exfoliated BC-N while slight deterioration occurred in BC-B nanohybrid. Further, the usual two

stage degradation for PMMA has been observed for pure bone cement and all nanohybrids arising from the side chain as well as main chain degradation of polymer molecules.[45] The T_g through DSC have been measured to be 98 ± 2, 101 ± 2 and 108 ± 2 °C for BC, BC-B and BC-N, respectively, exhibiting considerable higher relaxation temperature (~10 ^oC) in BC-N nanohybrid due to hindered structure in presence of homogeneous distribution of nanoclays arising from stronger interfacial interaction (supplementary Fig. S2). In case of BC-B nanohybrid, T_g value is close to pure bone cement suggesting insignificant interactions between polymer and silicate layers eventually unable to affect the segmental motion of polymer chains in bulk.

Mechanical properties of bone cement and its nanohybrids have been measured through tensile testing. The stress-strain curves have been presented in Fig. 3a showing better stiffness (slope of initial linear region) and toughness (area under stress-strain curve) of nanohybrids vis-à-vis pure bone cement. Amongst the nanohybrids, BC-N exhibits superior behavior as compared to BC-B both in terms of initial slope and elongation at break. The Young's modulus and toughness, a measure of energy required for breakage of material, have been shown in a bar diagram (Fig. 3b) indicating increase of modulus by 76 % ($p < 0.001$) and 82 % ($p < 0.001$) for BC-B and BC-N, respectively, in presence of rigid nanofillers with high tensile modulus showing very strong reinforcing effect of both the nanofillers. Further, significant improvement of toughness has been recorded in toughness of BC-N nanohybrid (~70 %) ($p < 0.001$) as compared to that of pure bone cement against almost similar toughness for BC-B nanohybrid primarily due to the greater interaction and homogeneous distribution of the nanoclay in BC-N by suppressing the crack growth mechanism by clay orientation towards stress field being strongly attached to the polymer chains.[46] It is worthy to mention that tensile properties (both stiffness and toughness) do exhibit composition dependency showing optimum properties for 1

wt% nanofiller containing nanohybrids, prompted us to use the particular composition throughout the whole studies. Kwon, S. Y et al,[27] reported decreasing order both for the compressive and tensile strength continuously with increasing filler concentration while this work categorically showing a optimum value at 1 wt% filler content with much higher tensile strength (~60 MPa) presumably because of enhanced interactions of organically modified nanocaly especially NK75 with polymer rich bone cement.

Fatigue resistance is an important consideration for any implant material to determine its self-life followed by another surgery to remove the implant. Comparative fatigue resistance (life) of nanohybrids with respect to commercial bone cement has been evaluated using a specially designed specimen, which mimic human hip prosthesis. For every category, two best metallic stem implanted femur specimens have been selected for fatigue testing under varying compressive loads starting from 1 kN to higher levels (up to failure point) at a frequency of 3Hz (stress control system) subjected to 50 k cycles at each level of applied compressive load. The details of the measurement have been presented in supplementary document (Fig. S3). Both pure bone cement and BC-B as grouting materials covering implants failed at 3.5 kN at 10k and 48k cycles, respectively, after passing the lower loads with the increment of 0.5 kN (Fig. 3c). Interestingly, BC-N as grouting material sustained compressive load of 4 kN and failed at a very high load of 4.5 kN at 1800 cycles. In order to determine the direct self-life in a single load and to compare the fatigue behavior, assessment has been performed at a particular compressive load of 3.5 kN (much higher than the load applicable for normal walking of human body at 70 kg weight; 2.1 kN) exhibiting 15 k, 120 k and 370 k cycles for pure BC, BC-B and BC-N nanohybrids, respectively, clearly indicate a dramatic improvement in fatigue resistance of BC-N nanohybrid as compared to BC and BC-B (Fig. 3d). To understand the mechanism of this

superior fatigue resistance, the surface morphology of the fractured zones has been analyzed. It shows smooth crack surface with higher fatigue crack growth for PMMA based pure bone cement, as expected from a brittle polymer revealing the propagation of crack steadily up to end point,[47] against compact and rough crack surface with discontinuous irregular markings and lower fatigue crack growth showing a typical morphology in BC-N (Fig. 3e) arising from strong interaction between the propagation crack and the nanoparticles with reduced growth of the propagating crack. The fracture morphology shows features like typical fatigue striations observed in metallic materials. The intimate interaction in case of BC-N is easily envisaged presumably due to hydrophobic interaction between hydrophobic PMMA and (dimethyl dihydrogenated tallow) ammonium modified nanoclay (NK75) as opposed to the weak van der Waals type of forces operative in BC-B occurring from the polar (methyl tallow bis-hydroxyethyl quaternary ammonium) organically modified nancolay (30B) and hydrophobic polymer (Fig. 3f). The closely associated polymer and nanoclay in BC-N help in transferring the stress caused by static and dynamic loading and, thereby, circumvent the catastrophic brittle failure occuring in pure bone cement. Thus, it is clear from these results that the BC-N has significantly higher fatigue resistance under cyclic loading as compared to the pure bone cement or BC-B nanohybrid. Further, both steady and dynamic measurements indicate greater mechanical strength of BC-N with respect to commercial bone cement and BC-B nanohybrid. It is and concluded that BC-N nanohybrid is definitely a better option to replace the commercial bone cement in total joint replacement for longer survival from mechanical point of view.

2.3 Biocompatibility:

Direct contact of any foreign material (implant) with blood may create hemolysis and the permissible limit of hemolysis for a biomedical implant should be less than 5 % [48] or, in other words, the extent of hemolysis reflects the bio-incompatibility of any implant. Hemolysis of ACD blood with heparinised films of BC-B and BC-N were shown 2.8 ± 0.3 and 2 ± 0.4 % ($p \leq 0.01$), respectively, with respect to BC (3.6 ± 0.3) indicating the nanohybrids to be better hemocompatible (Fig 4a).

In vitro osteoconductivity / bioactivity in terms of cell attachment and cell proliferation are essential modules to determine the biocompatibility of implant material. Human osteoblast like cells (MG-63) which produce phenotypic osteoblast markers and growth factors[49] have been used on the specimens of pure bone cement and its nanohybrids for cell adhesion through crystal violet assay. Optical densities were found to be 0.54 ± 0.1, 0.6 ± 0.11 and 1.02 ± 0.18 in BC, BC-B and BC-N ($p \leq 0.01$), respectively, with respect to control (0.4 ± 0.15 %) indicating seeding of cells occurs in great extent in BC-N (Fig. 4b). Seeding of cells and their relative quantity adhered on to various matrices has also been confirmed through surface morphology (supplementary Fig. S4) with rounded cell morphology on pure BC and BC-B nanohybrid with few of them are properly spread out while the cells attached largely on BC-N are properly spread on the surface holding tightly, clearly signifying strong cell adhesion on BC-N matrix as compared to other specimens leading to graphical illustration of cell adhesion as in Fig. 4c, where greater and healthier cell seeding takes place in more biocompatible and exfoliated (detached layers of nanoparticles) NK75 filler in BC-N nanohybrid as compared to less biocompatible and stacked layers of silicate in BC-B nanohybrid.

Further, MG-63 cell viability on bone cement and its nanohybrids have been examined through MTT assay at different time interval and the viability of the cells seeded on tissue culture plate surface was taken as the control. The cell viability was found to be ~80 ± 2 % for pure bone cement and BC-B after 1 day of incubation, while it was 95 ± 2 % ($p \leq 0.001$) for BC-N indicating superior cell viability in BC-N nanohybrid (Fig. 4d). Moreover, there is significant improvement in cell viability in BC-N after 5 days of incubation against no considerable change observed for pure bone cement and BC-B systems, and instead a slight deterioration has been noticed in BC-B nanohybrid as a function of time. The relative cell viability of different matrices has also been confirmed through fluorescence image of MG-63 cell proliferation on the support matrix during MTT assay measurement exhibiting the live cell density (per μm^2) of 60 ± 3, 30 ± 2, 12 ± 1 and 75 ± 3 for control, BC, BC-B and BC-N, respectively, (Fig. 4e) clearly shows much greater cell growth on BC-N as compared to others. In essence, the results have been attributed BC-N as highly biocompatible and bioactive material vis-à-vis commercial bone cement as well as BC-B nanohybrid.

***In vivo* studies:**

Understanding the biocompatible and bioactive nature of the developed nanohybrid especially BC-N, we implanted the material in vivo to discern the effect on bone healing. The right tibia of rabbit has been drilled to make cavity of 4 mm diameter to fill pure bone cement/ nanohybrids / control (no filling system) and post surgery healing process has been investigated through X-ray radiographic imaging, being a precise diagnosis technique for pre- and post-surgery bone fracture analysis. In control group (without any support), the cavities have been healed in ~ 90 days of post surgery (the position has been indicated by the arrows in Fig. 5) while pure bone cement filled cavities have been healed in ~60 days time, showing bit

improvement and emphasize the use of conventional bone cement for orthopedic surgery. Very interestingly, our developed nanohybrid (BC-N) could completely healed the similar cavities just in 30 days of time against pronounced infection observed using BC-B nanohybrid as the filling material as evident from the even bigger cavities remained after 140 days of surgery. Thus, in vivo radiographic experiment convincingly proves the efficacy of BC-N nanohybrid towards bone healing vis-à-vis conventionally used pure bone cement. In other words, calcium deposition was under the natural path in control systems to fill the cavity, while biologically inert bone cement has shown limited calcium deposition or bone connectivity on the bone cement surface. NK-75 reinforced nanohybrid (BC-N) has shown extensively enhanced bioactivity through cell growth on grouting material surface for healing of the bone. Subsidiary experiment of hydroxyapatite (HAP) deposition on different matrices using SBF (simulated body fluid) also confirm the relative amount of calcium in the order of BC-N > BC-B > BC through SEM micrographs and EDAX analysis exhibiting 8.4, 14.3 and 24.5 % of calcium on BC, BC-B and BC-N, respectively (Supplementary Fig. S5). Another vital component of HAP (phosphorous) formation also shows the similar trend indicating formation of HAP, essential constituent of bone, getting facilitated enormously on BC-N matrix as compared to pure bone cement or BC-B nanohybrid.

Histopathology:

Histopathology has been performed for the evaluation of bioactivity / osteoconductivity of bone cement and its nanohybrids through simultaneous examination on reformed bone and surrounding muscle tissues at the implant site using hematoxylin and eosin staining. Bone cement being well known (CMW1) bio-inert material, no new bone could be formed on pure bone cement even after 60 days of post surgery while good quality as new bone has been formed

in just 30 days of time in between the old bone and BC-N as filling agent (Fig. 6a). Since the cell density of the osteoblasts was high and osteoclasts was low, top right image of Fig. 6a of BC-N implanted histology shows the cell migration of osteoblasts towards the nanohybrids revealing superior osteoconductive nature which again clearly substantiate in bone remodeling observed after 60 days showing good number of osteocytes and osteoclastes in the case of BC-N nanohybrid. In contrast, malignancy occurs in BC-B implanted rabbit tibia which gets aggravated with time (60 days) supporting the radiographic in vivo experiment. It is to be noted that meager new bone formation has been observed after 60 days in control system (without any support; natural system) as noticed in the right lower image of Fig. 6a. Moreover, the histopathology of the surrounding muscle tissue near the implanted bone cement/ hybrids/ control site show (Fig. 6b) some malignant debris found on pure bone cement, presuambly due to cell necrosis during T_{max}, thorough dead tissue debris on BC-B, due to strong infection at implanted area while healthy tissues are observed on BC-N, predominantly due to better biocompatibility along with the reduced exothermic temperature in case of BC-N nanohybrid as reported in Fig. 4 and 2a, respectively. Hence, it is conclusively proven that the BC-N nanohybrid, being highly bioactive and biocompatible, is well tested for its significantly greater efficiency for bone healing than that of commercial bone cement without side effect, advancing the use of hybrid substance as grouting material especially for bone healing.

The argument of behaving with large dissimilarity by the two different layered silicates is required to be understood for better design of material where origin (chemical composition) and the nature of surface modifications of the nanoclays are different. The elemental analysis through EDAX of the two nanoclays show the considerable differences in their constituents (Mg, Al, Si, Fe and Cu with 0.7, 22, 32, 7.1 and 0.3 wt%, respectively) in NK75 organoclay against similar

sequence of elements as 2.5, 19, 33, 2 and 0.1 wt% in 30B organoclay (Supplementary Fig. S6) indicating major alteration of chemical composition of Mg and Fe in two different nanoclays (30B: 2.5 % Mg, 2 % Fe and NK75: 0.7 % Mg, 7.1 % Fe) suggesting Mg rich 30B vis-à-vis Fe rich NK75 nanoclays. Therefore, it is pertinent to look into the elemental influence on bioactivity / biocompatibility.

Elemental effects and surface modification on biological responses:

Cell viability through MMT assay has been performed for a series of salt concentration separately for Mg and Fe ion containing salt to understand the bioactivity / biocompatibility of the individual element initially and the concentrations are so chosen which reflect the quantity of the respective ions present in two nanoclays mentioned above. The percentage of cell viability systematically increases with higher concentration of Fe containing salt (Fig. 7a). On the other hand, cell viability consistently decreases for higher concentration of Mg ion containing salt (Fig. 7b), clearly indicating the enhanced bioactivity (in terms of cell proliferation) in presence of higher Fe content solution while Mg deteriorates the biocompatibility at higher concentration. The fluorescence images at varying concentrations also support the relative cell growth for two different salts separately (inset images of Fig. 6 a & b at 5 days of incubation time for every cases). As the real nanoclays contain both Fe and Mg ions, two salt solutions (Fe + Mg) mimicking those concentrations corresponding to nanoclays have also been prepared and their bioactivities have been performed showing marginal increase in cell proliferation as a function of time related to the composition corresponding to NK75 nanoclay while cell viability significantly decreases at longer period of time for the mixture of salt solution equivalent to the composition of 30B nanoclay (Fig. 7c) clearly indicating bioactive nature of chemical composition corresponding to NK75 nanoclay against the toxic nature of the chemical composition mixture

related to 30B nanoclay. Cell morphology through fluorescence imaging also supports the exactly similar trend of cell growth for two different mixtures of solutions corresponding to NK75 and 30B nanoclays after 5 days of incubation in culture medium showing larger number of cells in 8% Fe + 1 % Mg (~ NK75 composition) as compared to 2 % Fe + 2.5 % Mg (~30B composition) (inset of Fig. 7c). Moreover, the health of the growing cells has been monitored on NK75 and 30B nanoclays as supports after one day of incubation time indicating large number of cell death (red colored cells / red nucleus depending on the early or late apoptosis) on 30B nanoclay against mostly healthy cells (green colored cells) on top of NK75 strongly suggesting that NK75 facilitates the cell proliferation while 30B nanoclay worsen the cell health leading to apoptosis (Fig. 7d & e). The details of apoptosis behavior in different concentrations of Fe and Mg solutions after proper staining have also been presented in supplementary Figure S6 to understand the relative cell health in two different ions at varying concentrations. However, it is evident that higher concentration of iron is more bioactive while larger amount of magnesium reduces the bioactiveness considerably.

Iron being an essential constituent of many biological molecules/cells, it has major advantages for its use as implant material in terms of interactions with organism and has a window limit of 10 µg/ml for which the metabolic activity of endothelial cells enhances steadily followed by its lower efficiency at very high concentration.[50-52] In BC-N nanohybrid, the approximate iron content was 400 µg and considering the amount of blood in rabbit ~ 200 ml in general, the iron concentration would be nearly 2 µg/ml providing a favorable condition for bone cell proliferation in BC-N as compared to bio-inert pure bone cement (in absence of any iron). In addition, iron is highly bioactive and has an ability to nucleate the apatite with faster rate.[52] Further, the cell viability is reported to be decreased with increasing cation exchange capacity

(CEC) of nanoclay[53] and NK75 having lower CEC as compared to 30B nanoclay is primarily responsible for higher cell viability in BC-N than that of BC-B. Moreover, human (osteoblast) cell membrane surface is negatively charged, primarily due to carboxylates and phosphates ions present in proteins and glycans,[54] and therefore, it has a natural tendency to be attracted by the positively charged layered silicate facilitated by the electron accepting and donating capability of iron in its inter-conversion of $Fe^{+2} \leftrightarrow Fe^{+3}$.[51] Usually, montmorillonite type layered silicates promote bioactivity[55] and higher percentage of iron in NK75 further improves the biocompatibility and cell proliferation. On the contrary, even though the magnesium is known to be biodegradable but its leaching at higher concentration produce cyto- and genotoxic effects after internalization presumably through the increases of pH and hydrogen evolution[56] causing infection in BC-B nanohybrid or apoptosis of cell using control experiment with magnesium ion alone. However, we have chosen the right nanoclay which contains most favorable elemental composition, and thereby, showing the quickest ever bone healing using the nanohybrid of bone cement. Surface modifications of the layered silicates also help improving the biological activity of the composite as revealed from the lowering of contact angle (75^o and 73^o for BC-N and BC-B, respectively, as compared to 81^o for pure bone cement) thereby increasing the hydrophilic nature of the overall composite facilitate the cell growth in composite vis-à-vis pure bone cement. The lowest contact angle for BC-B arises from the polar organic modification on top of silicate surface while its higher magnesium content in silicate deteriorates largely the cell growth in BC-B. However, a superior bone healing nanohybrid has reported for practical use as implant in joint surgery with proven mechanical and biological properties.

CONCLUSIONS

Novel nanohybrid of bone cement has been prepared with nanoclays by varying the chemical composition of layered silicates as well their surface modification. The mixing temperature, resulting from exothermic polymerization, in nanohybrid (BC-N) has been reduced by 12 ^{o}C as compared to pure bone cement (84 ^{o}C), diminishing the chances of cell necrosis for the use of nanohybrid as implant material. The thermal stability of the nanohybrid (BC-N) has enhanced by 30 ^{o}C along with higher stiffness and toughness as measured from the area under the stress-strain curve as compared to that of pure bone cement. The fatigue resistance of the nanohybrid (BC-N) increases significantly both under varying and constant dynamic load at fixed frequency making the material more suitable as possible grouting material in joint surgeries. The cause of improvement in the properties has been explored and found to be greater interaction between the components (BC and NK75) is responsible for these behaviors as compared to the less interactive system with BC and 30B in BC-B nanohybrid. The biocompatibility/ bioactivity of the nanohybrids have been verified and found supplementary bioactive nature of BC-B as compared to pure bone cement against the deteriorating nature of BC-B as a function of time. The comparative bone healing capability have been investigated using bone cement and its nanohybrid as grouting material in vivo clearly exhibiting the superior healing power of BC-N nanohybrid (one-third time with respect to pure bone cement) against the highly infectious nature using BC-B. The histopathology of bone also supports the radiographic experiment showing new bone formation using BC-N in just 30 days time against 90 days in case of pure bone cement and cell malignancy in BC-B nanohybrid. Similar situation prevails for muscle histopathology as well. The cause of much dissimilarity using two different nanoclays has been work out on the basis of the elemental composition through cell culture and found that

higher percentage of iron in the nanoclay (NK75) helps improving the biocompatibility and larger quantity of magnesium depreciate the bioactivity of nanoclay (30B). In brief, a novel nanohybrid (BC-N) has been developed and found much appropriate as a new class of grouting materials, in terms of implantation, mechanical and biological aspects, for total joint surgery vis-à-vis the conventional bone cement used at present.

Supporting Information Available: This material is available free of charge via the Internet at http://pubs.acs.org

ACKNOWLODGEMENT

The author (Govinda Kapusetti) gratefully acknowledges financial support from the Council of Scientific and Industrial Research (CSIR), Government of India in the form of fellowship. The authors are thankful to Dr. S. K. Singh, Centre for Animal Surgery and Medicine and Dr. A. Dwivedi, Department of Radiology, IMS, BHU for their help in this work**.** The authors acknowledge the help of Mr. Sashank Mishra, lab attendant, Centre for Animal Surgery and Medicine, IMS, BHU for his help in histopathology studies. The authors also acknowledge the support of Dr. D.K. Avasthi, Mr. P. K. Kulriya of IUAC, New Delhi for XRD measurements and Dr. S. Malik and Mr. Chanchal Chakraborty of IACS, Kolkata for TEM studies.

References

[1] Bayston, R.; Milner, R. D. *J. Bone Joint Surg. Br* **1982**, *64*, 460–464.

[2] Dunne, N. J.; Orr, J.F. *J. Mater. Sci: Mater. Med*. **2002**, *13*, 17–22.

[3] Wang, J. S.; Franzen, H.; Toksvig-Larsen, S.; Lidgren L. *J. Appl. Biomater.* ***1995***, *6*, 105–108.

[4] Freeman, M. A.; Bradley, G. W.; Revell, P. A. *J. Bone Joint Surg. Br.* **1982**, *64*, 489–493.

[5] Jasty, M.; Maloney, W. J.; Bragdon, C. R.; Haire, T;, Harris, W. H. *J. Bone Joint Surg. Am.* **1990**, *72*, 1220–1229.

[6] Kuehn, K. D.; Ege, W.; Gopp, U. *Orthop. Clin. North Am.* **2005**, *36*, 17–28.

[7] Jasty, M.; Maloney, W.; Bragdon, C. R., O'connor, D.; Haire, T.; Harris, W. H. *J. Bone Joint Surg.* **1991**, *73*, 551–558.

[8] Vallo, C. I.; Abraham, G. A.; Cuadrado, T. R.; San, R. J. *J. Biomed. Mater. Res. B Appl. Biomater.* **2004**, *70*, 407–416.

[9] Chao, F.; Feibin, ; Yang, C.; Jun, F.; Ya-Jun C. *J. Mater. Chem. B* **2013**, *1*, 4043-4048.

[10] Marrs, B. Carbon nanotube augmentation of a bone cement polymer. Ph.D. Dissertation, University of Kentucky, USA, **2007**.

[11] Tsukeoka, T.; Suzuki, M.; Ohtsuki, C.; Sugino, A.; Tsuneizumi, Y.; Miyagi, J.; Kuramoto, K.; Moriya, H. *Biomaterials* **2006**, *27*, 3897–3903.

[12] Blanca, V.; Maria, P. G.; Xavier, G.; Josep, A. P.; Julio, S. R. *Biomaterials* **2005**, *26*, 4309–4016.

[13] Puska, M. A.; Kokkari, A. K.; Narhi, T. O.; Vallittu, P. K. *Biomaterials* **2003**, *24*, 417–425.

[14] Pourdeyhimi, B.; Wagner, H. D. *J. Biomed. Mater. Res.* **1989,** *23*, 63–80.

[15] Kim, H.Y.; Yasuda, H.K. *J. Biomed. Mater. Res.* **1999**, *48*, 135–142.

[16] Saha, S.; Pal, S. *J. Biomed. Mater. Res.* **1983**, *17*, 1041–1047.

[17] Shinzato, S.; Kobayashi, M.; Mousa, W. F.; Kamimura, M.; Neo, M.; Kitamura, Y.; Kokubo, T.; Nakamura, T. *J. Biomed. Mater. Res.* **2000**, *51*, 258–272.

[18] Vallo, C. I. *J. Biomed. Mater. Res.* **2000**, *53*, 717–727.

[19] Knoell, A.; Maxwell, H. *Analy. Biomed. Engg.* **1975**, *3*, 225–229.

[20] Misra, N.; Kapusetti, G.; Jaiswal, S.; Maiti, P. *J. Appl. Poly. Sci.* **2011**, *121*, 1203–1213.

[21] Kapusetti, G.; Misra, N.; Singh, V.; Kushwaha, R.K.; Maiti, P. *J. Biomed. Mat. Res. A* **2012**, *100*, 3363–3373.

[22] Kapusetti, G.; Mishra, R. R.; Srivastava, S.; Misra, N.; Singh, V.; Roy, P.; Singh, S. K.; Chakraborty, C.; Malik, S.; Maiti, P. *J. Mate. Chem. B* 2013, *1*, 2275–2280.

[23] Wang, C. X.; Tong, J. *Bio-Med Mate Engi.* **2008,** *18*, 367–375.

[24] Hill, J.; Orr, J.; Dunne, N. *Int. J. Nano Biomat.* **2008** , *1*, 237 – 249.

[25] Hill, J.; Orr, J.; Dunne, N. *Int. J. Nano Biomat.* **2007**, *1*, 138 – 153.

[26]Wang J-H, Young T-H, Lin D-J, Sun M-K, Huang H-S, Cheng L-P. *Macromol. Mater. Eng.* **2006**, *291*, 661–669.

[27] Kwon, S. Y.; Cho, E. H.; Kim, S. S. *Macromol. Symp.* **2007**, *249-250(1)*, 86-95.

[28] Deka, M.; Kumar, A. *Electrochimica Acta* **2010**, *55* 1836–1842.

[29] Boumbimba, R. M.; Ahzi, S.; Bahlouli, N.; Ruch, D.; Gracio, J. *J. Engg. Mater. Tech.* **2011**, *133*, 30908–309111

[30] Miroslav, H.; Majda, Z. *Euro. Poly. J.* 2007, *43*, 4891–4897.

[31] Si, M.; Goldman, M.; Rudomen, G.; Gelfer, M. Y.; Sokolov, J. C.; Rafailovich M. H. *Mater. Eng.* **2006**, *291*, 602–611.

[32] Costache, M. C.; Wang, D.; Heidecker, M. J.; Manias, E.; Wilkie, C. A. *Adv. Technol.* **2006,** *17***,** 272–276.

[33] Sarkar, M.; Dana, K.; Mukhopadhyay, T. K.; Ghatak, S. *Trans. Ind. Ceram. Soc.* **2011**, *70***,** 23-28.

[34] Storer, R. A. editor. *Standard specification for acrylic bone cement*. *Ann. Book ASTM Stand* 199, F451-99a, 13.01:56.

[35] Amos, R.; Mark, A. M.; Kenneth, A. M. *J. Biomech.* **2008**, *41*, 3017–3023.

[36] Kueng, W.; Silber, E.; Eppenberge, U. *Anal. Biochem.* **1989**, *182*, 16–9.

[37] Castaldini, A.; Cavallini, A. *Biomaterials* **1985**, *6*, 55–60.

[38] Lin, X. *Analysis and Identification of Infrared Spectrum of the Polymer;* University Press: Chengdu, China, **1989**.

[39] Shafee, E.E. *Polym. Degrad. and Stab.* **1996**, *53*, 57–61.

[40] Lopes, P.; Corbellini, M.; Ferreira, B.L.; Almeida, N.; Fredel, M.; Fernandes, M.H.; Correai, R. *Acta Biomater.* **2009**, *5*, 356–362.

[41] Choy, J.H.; Jung, J.S.; Oh, J.M.; Park, M.; Jeong, J.; Kang, Y.K.; Han, O.J. *Biomaterials* **2004**, *15*, 3059–3064

[42] Deka, M.; Kumar, A. *Electrochimica Acta* **2010**, *55* 1836–1842

[43] Miroslav, H.; Majda, Z. *Euro Poly J* **2007**, *43*, 4891–4897.

[44] Wang J-H, Young T-H, Lin D-J, Sun M-K, Huang H-S, Cheng L-P. *Macromol. Mater. Eng.* **2006**, *291*, 661–669

[45] Costache, M. C.; Wang, D.; Heidecker, M. J.; Manias, E.; Wilkie, C. A. *Polym. Adv. Technol.* **2006,** *17***,** 272-276.

[46] Saha, D.; Maiti, P.; David, J.J.; Carl, A.B.; Emmanuel, P. G. *Adv. Mater.* **2005**, *17*, 525–528.

[47] Kwon, S. Y.; Cho, E. H.; Kim, S. S. *Macromol. Symp.* **2007,** 249-250(1), 86-95.

[47] Benvenuti, E.; Tovo, R.; Livieri, P. A. *Fratturaed Integrità Strutturale* **2011,** *17*, 23-31.

[48] Rusu, M.C.; Ichim, I.C.; Popa, M.; Rusu, M. *J. Mater. Sci. Mater. Med*. **2008**, *19*, 2609–2617.

[49] Kieswetter, K.; Schwartz, Z.; Hummert, T.W.; Cochran, D.L.; Simpson, J.; Dean, D.D.; Boyan, B.D. *J. Biomed. Mater. Res.* **1996**, *32*, 55–63.

[50] Shengfa, Z.; Nan, H.; Li, X.; Yu, Z.; Hengquan, L.; Hong, S.; Yongxiang, L. *Mater. Sci. Eng. C* **2009,** *29*, 1589–1592.

[51] Matthias, P.; Carola, H.; Tirza S.; Christoph, F.; Philipp, B.; Christian von, S. *Biomaterials* **2006,** *27*, 4955–4962.

[52] Fujishiro, Y.; Sato, T.; Okuwaki, A. *J. Mater. Sci: Mater. Med.* **1995,** *6*, 172–176.

[53] Lin, F. H.; Chen, C. H.; Cheng, W. T.; Kuo, T. F. *Biomaterials* **2006**, *27*, 3333–3338.

[54] Bezanilla, F. *Nature Rev. Mole. Cell Biol.* **2008**, *9*, 323–332.

[55] Paluszkiewicza, C.; Wesełucha-Birczyn´skab, A.; Stodolak-Zychc, E.; Hasika M. *Vibr. Spectro.* **2012,** *60*, 185–188.

[56] Ana, L.; Di, V.; Miguel, R.; Ferna´ndez, M. L. M. *J. Biomed. Mater. Res. B* **2011,** *99***,** 111–119.

Figure 1

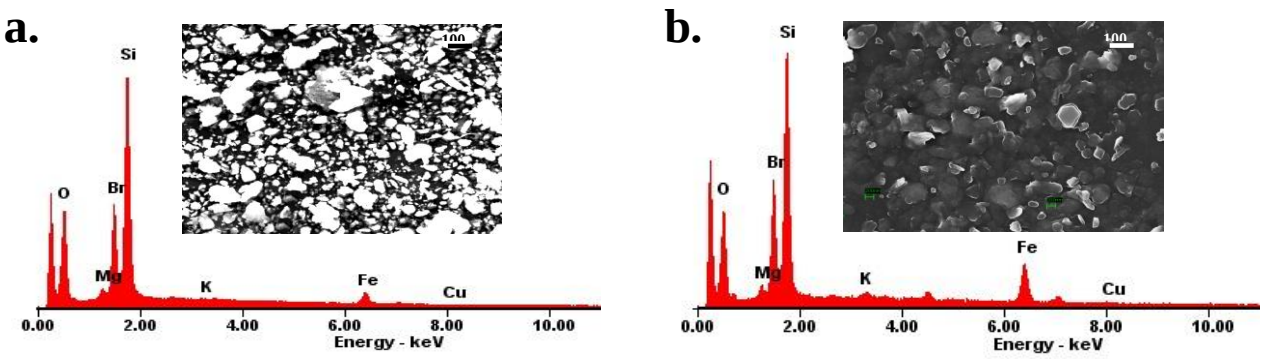

Figure 1: EDAX patterns show the elements present in (a) 30B and (b) NK-75 and the insert images show their respective morphology and relative particle size.

Figure 2

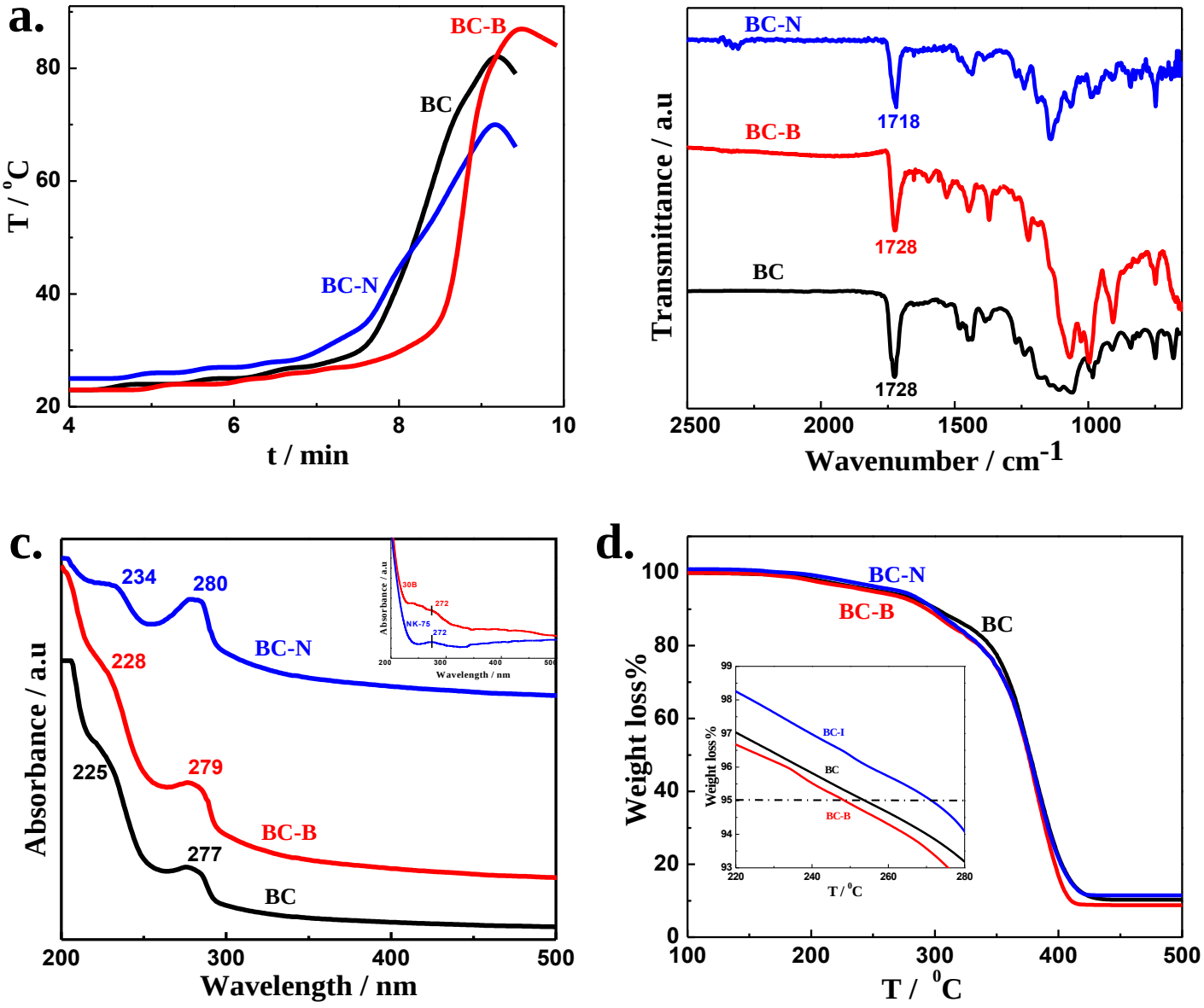

Figure 2: (**a**) Evolution of temperature as function of bone cement setting time of commercial bone cement (BC) and its 1wt% 30B (BC-B) and NK-75 (BC-N) nanohybrids, (**b**) FTIR spectra revealing functional groups and interactions in two different nanohybrids as indicated in, (**c**) UV-Vis spectra showing n → σ* and π → π* transitions in nanohybrids indicating the relative interactions and, (**d**) Thermal stability of nanohybrids against neat bone cement by measuring the of degradation temperature through thermal gravimetric analysis (TGA) (a) BC-0 and its 30B/NK75 nanohybrids. Insert figure shows the enlarged part of the temperature between 220 to 280°C indicating clear change in degradation temperature.

Figure 3

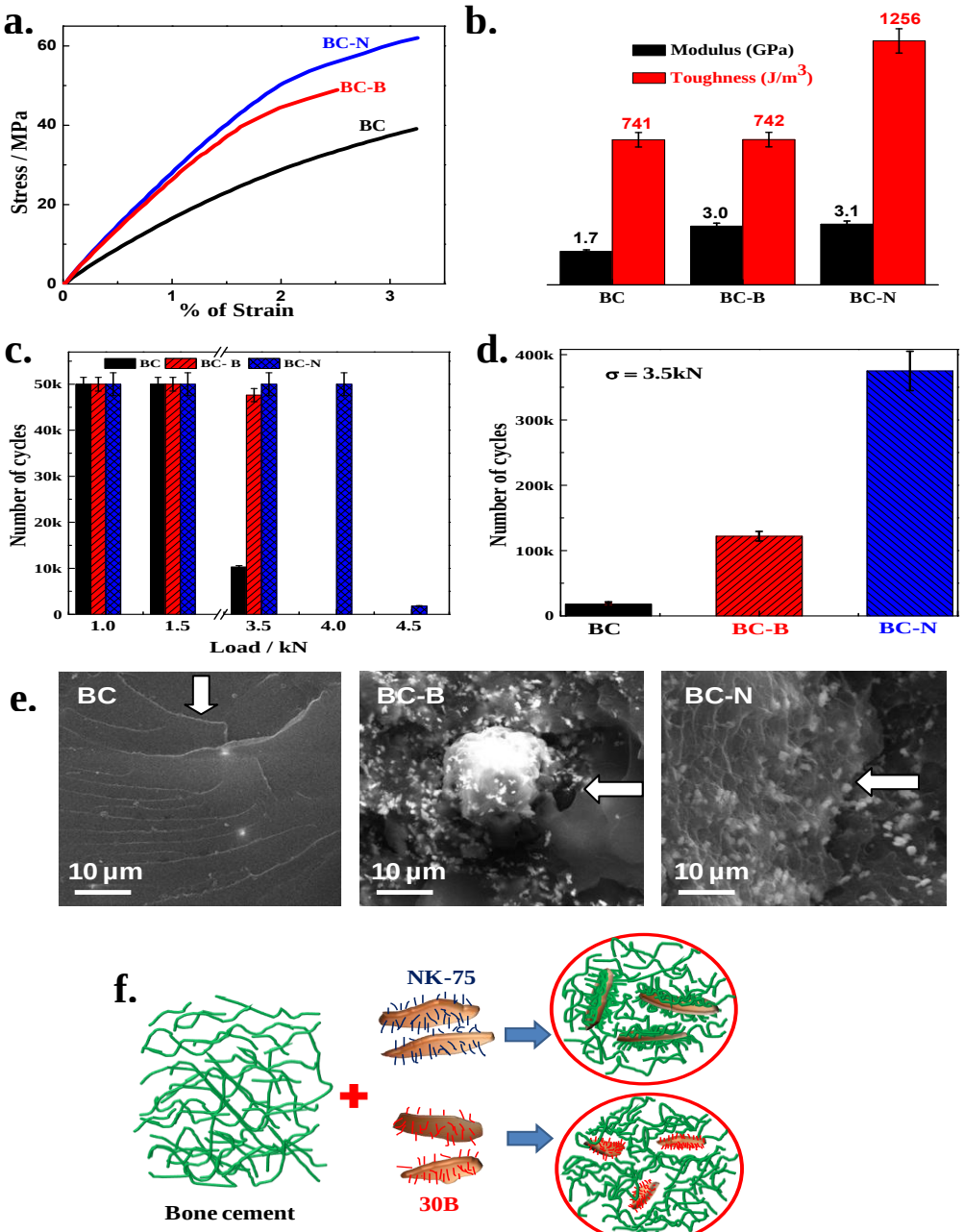

Figure 3: (**a**) Stress strain curves of bone cement (BC) and its nanohybrids (1 wt% filler concentrations), (**b**) Bar diagrams showing elastic modules and toughness of bone cement and its nanohybrids the number above the bar diagram indicate the actual values in respective units, (**c**) Bar diagram showing the fatigue life in terms of number of cycles for pure bone cement and its 1 wt% nanohybrids under varying applied loads as shown on X-axis, (**d**) Bar diagram s showing the fatigue resistance of bone cement and its nanohybrids in terms of cycles at a constant load (3.5kN), (**e**) Fracture surface morphology of BC, BC-B and BC-N after fatigue failure. Arrow marks indicate the direction of crack propagation and (**f**) Schematic representation of nanoclay and bone cement interactions which eventually responsible for stress transfer to indicate the failure behavior.

Figure 4

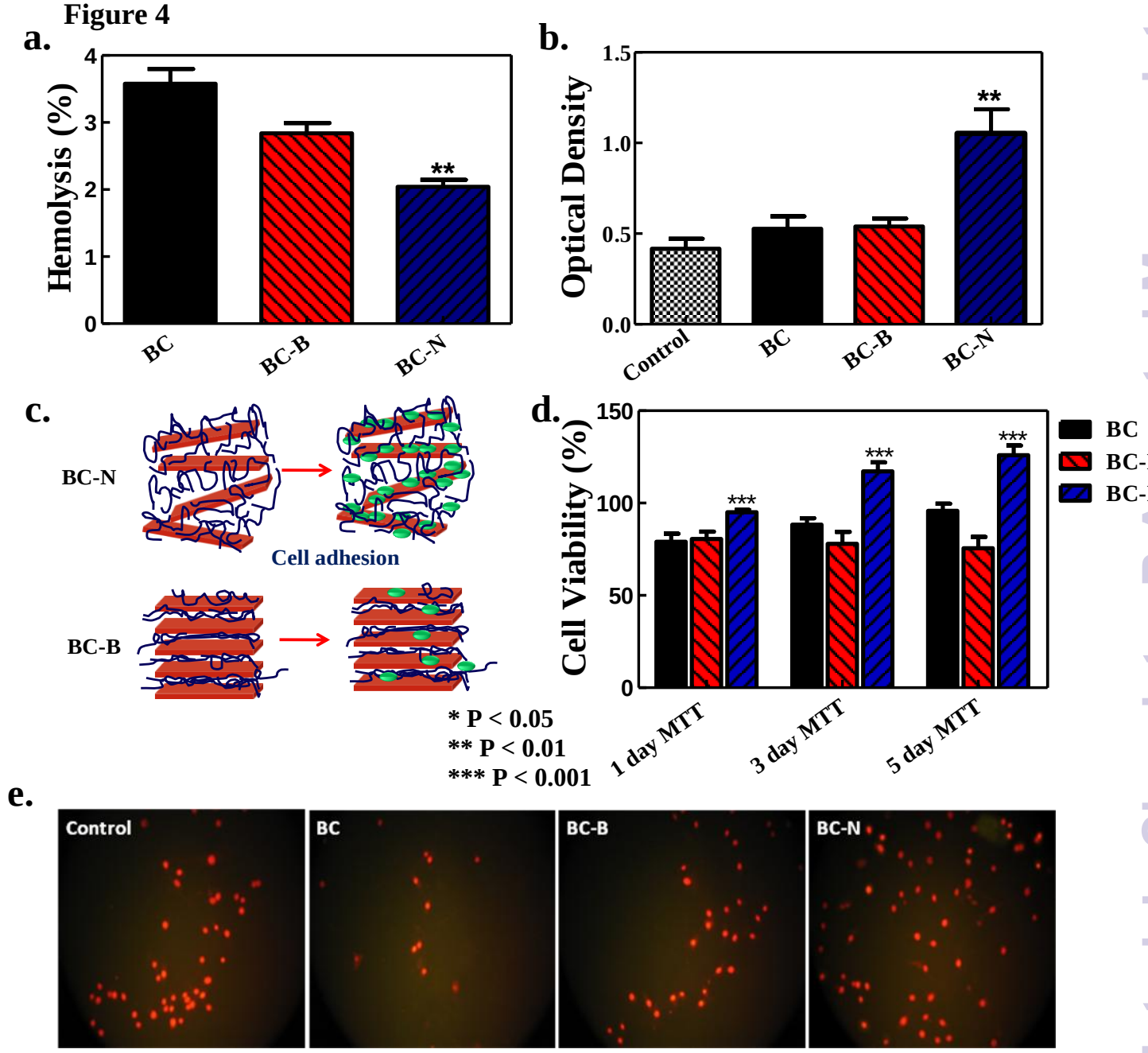

Figure 4: Biocompatibility evolution of bone cement and its nanohybrids (**a**) The bar diagrams show the percentage hemolysis in presence of bone cement and its two different nanohybrids suggesting insignificant hemolysis in nanohybrids, (**b**) MG-63 cell adhesion on bone cement and its nanohybrids in terms of optical density. The absorption values were taken at 570nm wave length, (**c**) Schematic representation of cell adhesion phenomenon on BC-B and BC-N, (**d**) MG-63 cell viability of bone cement and its indicated nanohybrids with time interval of 1, 3 and 5 days through MTT assay measurement showing better cell viability in BC-N and (**e**) Fluorescence images of cells cultured on bone cement and indicated nanohybrids after one day of cell proliferation, indicating superior cell growth in BC-N.

Figure 5

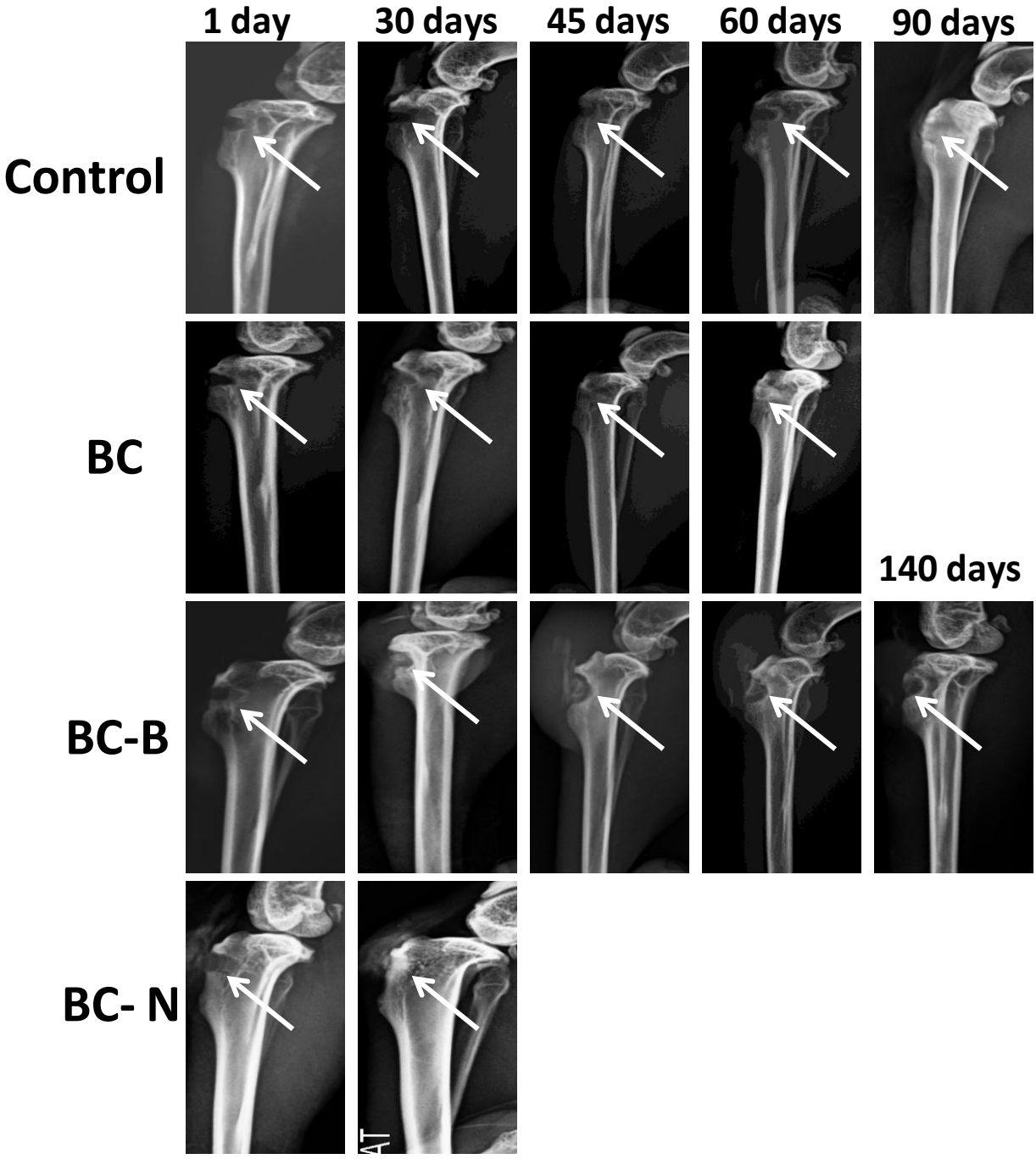

Figure 5: Post surgery X-ray images of rabbit tibia at time interval of 1, 30, 45, 60, 90 and 140 days after filling the holes with pure bone cement, BC-B and BC-N. The arrows indicate the position of hole during the course of time. Control images indicate the healing process as a function of time at the time without any supporting material (natural healing).

Figure 6

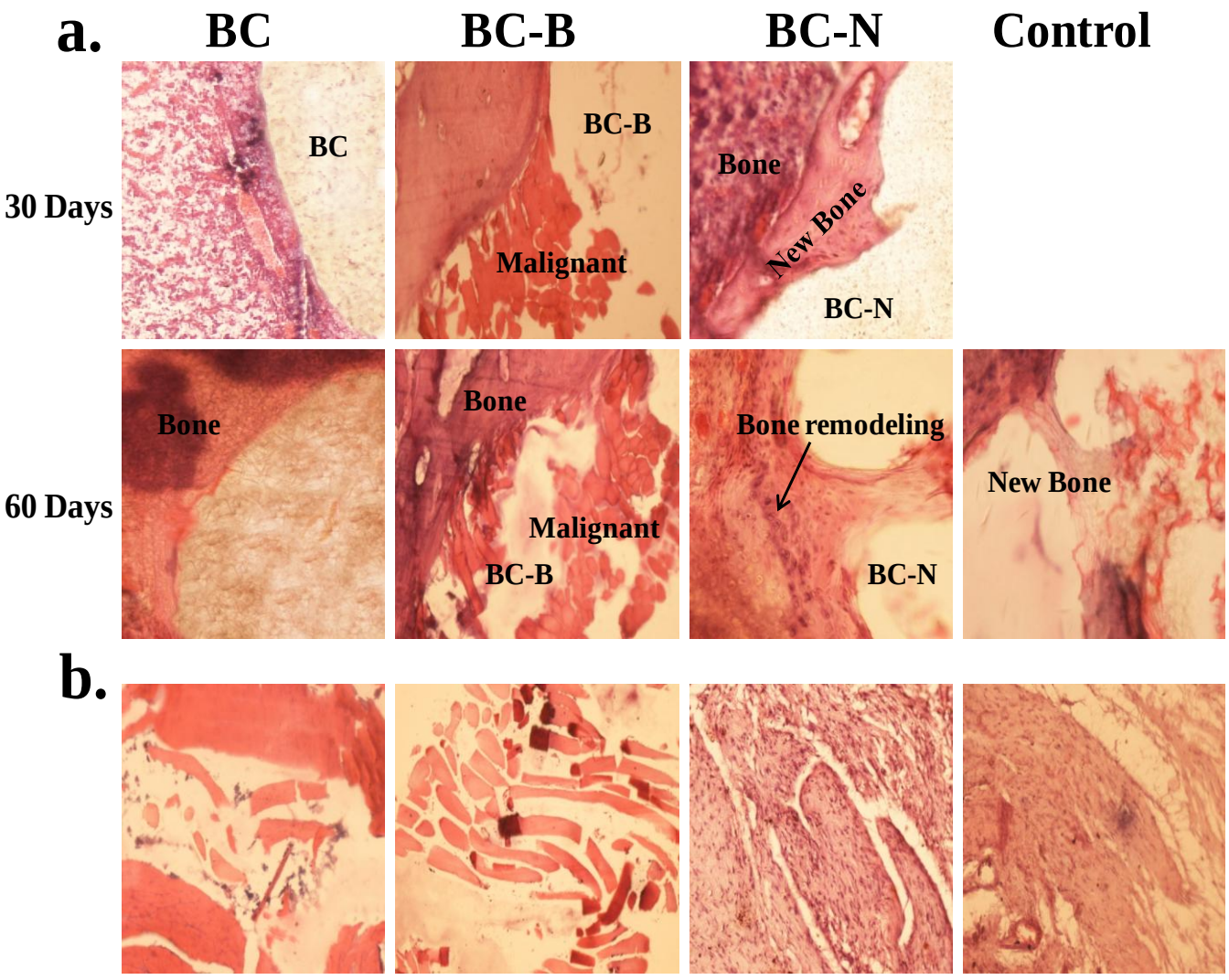

Figure 6: Hematoxylin and eosin staining histopathologcal images of (**a**) decalcified bone samples of rabbit tibia in the implanted site filled either with bone cement (BC) and BC-N have been compared with control (without any supporting material) after 30 and 60 days of post surgery showing infection in BC-B against excellent new bone function in BC-N and, (**b**) surrounding tissues of the implanted site after 60 days of post surgery indicated best possible cell growth on BC-N vis-à-vis infection with BC-B, while BC & control system exhibit normal behavior.

Figure 7

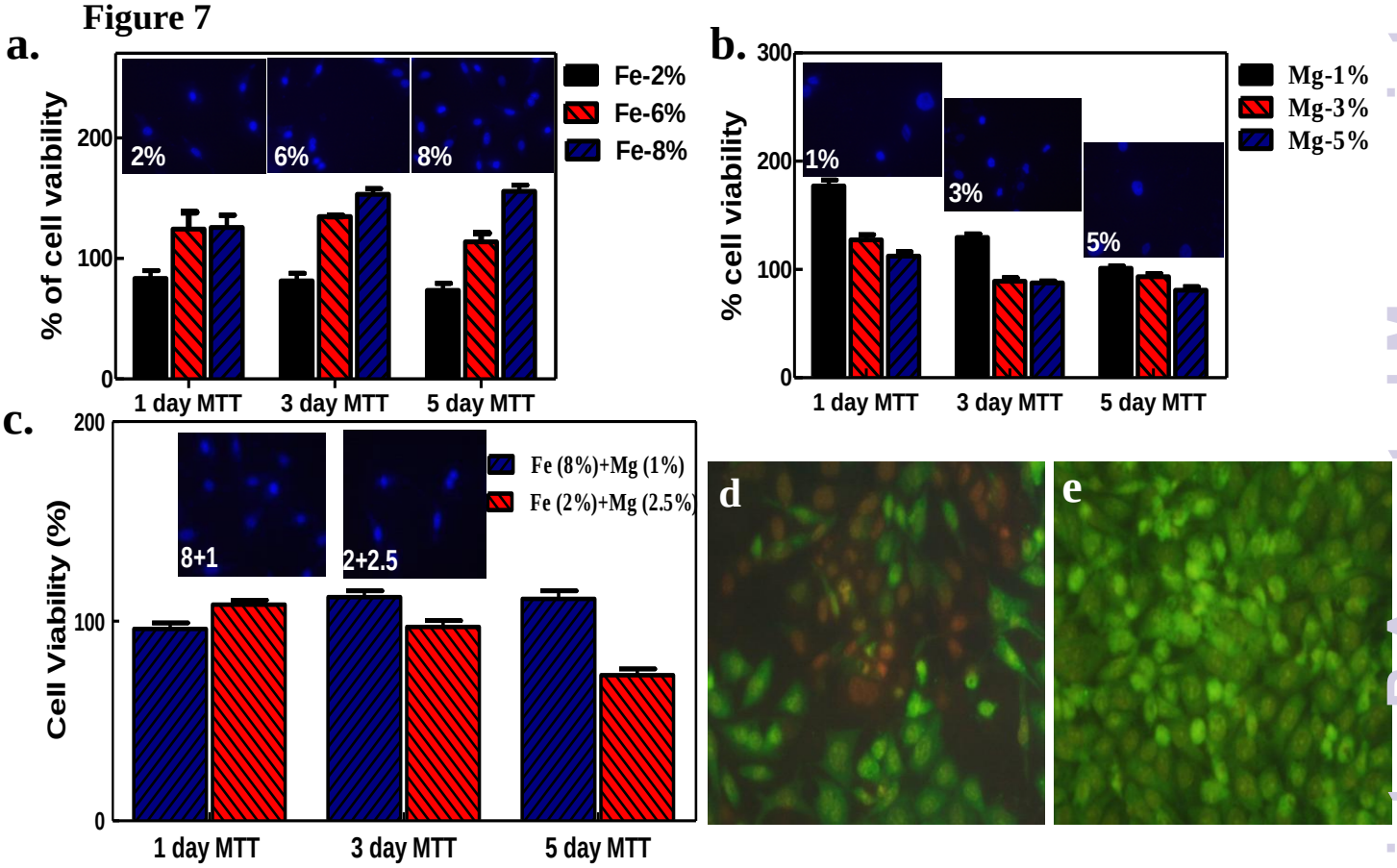

Figure 7: Cell viability as measured through MTT assay after 1, 3 and 5 days time and inserted images show the fluorescence staining of cell proliferation for 3 days incubation (**a**) Cell viability in Fe medium containing of Fe salt indicating greater cell growth at higher Fe content of 2, 6 and 8 wt%, (**b**) Cell viability in Mg medium containing Mg/salt suggesting reduced cell growth at higher Mg content of 1, 3 and 5wt%, (**c**) Cell viability of Fe and Mg ion containing systems mimicking compositions of two nanoparticles (NK-75 and 30B) revealing better cell growth in the concentration corresponding to NK-75 while reducing behavior is observed in the composition related to 30B clay and (**d&e**) cell apoptosis images in 30B and NK-75 mimicking systems, respectively (green-live cells, red- dead cells

Table of Content only

Bone cement based nanohybrid as super biomaterial for bone healing

Govinda Kapusetti[1], Nira Misra[1], Vakil Singh[2], Swati Srivastava[3], Partha Roy[3], Kausik Dana[4] and Pralay Maiti[5,*]

Novel bone cement nanohybrid has been developed with stiffer and tougher by design which heals the broken bone at a faster rate.